Finite element modelling of brittle fracture of thick coatings under normal and tangential loading

A.L. Mohd Tobi[a,b], P.H. Shipway[a], S.B. Leen[c]

[a] *University Technology Centre in Gas Turbine Transmission Systems, Division of Materials, Mechanics and Structures, University of Nottingham, University Park, Nottingham, NG7 2RD, UK.*

[b] *Faculty of Mechanical and Manufacturing Engineering, Universiti Tun Hussein Onn Malaysia, Batu Pahat, Malaysia.*

[c] *Mechanical and Biomedical Engineering, College of Engineering and Informatics, NUI Galway, Ireland.*

Received Date Line

Abstract

This paper addresses coating fracture in hard brittle coatings subjected to combined normal and tangential loads through a finite element based methodology. The coating is modelled as an elastic layer perfectly bonded to an elastic substrate with a pre-microcrack, assumed to initiate at the contact trailing edge due to high tensile stress. The predicted results are consistent with previously published coating fracture results. The model predicts a significant effect of coating thickness on crack propagation for coatings with large elastic mismatch and the final propagated crack profile is predicted to depend on friction coefficient, coating fracture toughness and sliding displacement.

Keywords: Brittle fracture, Coating, Finite element model

1. Introduction

Coatings have been widely used in engineering applications such as the automotive, manufacturing and aeroengine industries to increase the wear resistance of components and reduce friction on contact surfaces. With low levels of friction, components will experience lower stress magnitudes resulting in increased operational life. Increasing the wear resistance of coatings is often achieved through increased hardness which in turn reduces the rate of abrasion in the wear process. This however comes at the expense of coating brittleness and associated susceptibility to brittle-type fracture in practical applications [1].

In engineering applications, the ability of coatings to perform without catastrophic failure is a major concern. The failure of coated substrates can be related to the failure of coating itself or to the deformation of the substrate. Several different mechanisms of failure have been observed in hard-coated surfaces, such as through-thickness cracking, delamination, spallation and coating buckling [2, 3]. It has been observed, however, that hard-coated surfaces very often fail due to tensile fracture. Tensile fracture mainly occurs at the contact edge of a contact due to the high tensile stresses experienced there [4, 5]. Strawbridge and Evans [6] schematically presented the possible failure modes of coated substrates subjected to tensile stress as: (a) transverse cracking in the coating only, (b) transverse cracking in the coating and the substrate, and (c) transverse cracking followed by delamination. Shima et al. [7] have highlighted the role of the substrate in supporting load without unacceptable levels of deformation (commonly termed the load supporting ability) and its dependence upon factors such as substrate hardness and elastic modulus.

Contact stresses in layered contacts are reasonably well understood [8 - 10]. For a situation where the layer thickness is large compared to the contact size, the substrate has little influence on the stress distribution and the contact solution is well described by application of Hertz theory to the layer. The effect of surface roughness on layered surfaces has also been studied by Cole and Sayles [11], based on the contact configuration of Gupta and Walowit [10]. Work on modelling and simulation of a coated tribological contact with normal and tangential loading has been reported by a number of researchers [5, 12 and 13]; it was shown that the stresses within the layer varied with the level of elastic mismatch and with the coating thickness. Under normal and tangential loading, for a relatively thin, stiff coating on a compliant substrate, the tensile stress at the trailing edge has been shown to reduce with increasing coating thickness and vice versa for a compliant coating on a stiff substrate [12, 13].

Some previous work has addressed numerical analysis of brittle fracture under contact loading [14 - 16], demonstrating a strong dependence of fracture load on the elastic mismatch of the coating and substrate under normal and tangential loading. Holmberg et al. [5] modelled a 3-D scratch test of a TiN coated steel under elastic and plastic deformation and compared it with test results; the first crack observed in the tests is associated with the bending and tensile stresses at the top of the coating as it is slid against the indenter. Hills et al. [14] studied horseshoe cracks appearing behind a spherical indenter sliding along the surface of a brittle material. A model for transverse cracking observed during four-point bending of coated substrates was presented by Dalmas et al. [17], obtained by use of the integral equation method. Bansal et al. [18] carried out finite element (FE) modelling of the

fracture behaviour of HVOF sprayed WC-Co coatings in a four-point bending test, and described the effect of coating thickness, residual stress, and coating modulus on the fracture response in bending.

Since the majority of highly wear resistant coatings used in engineering applications (such as thermally sprayed coatings, e.g. [18]) are typically brittle in nature and susceptible to failure by tensile fracture, it is important to study the fracture behaviour of thick brittle coatings subjected to contact loading to assist in the process of coating design and selection. This paper presents an FE-based fast fracture crack growth simulation methodology for a coated substrate subjected to combined normal and tangential contact loading. The effects of elastic mismatch between the coating and substrate and the effects of coating thickness and contact friction on the fracture behaviour have been investigated.

2. FE model

2.1. Model description

Fig. 1a shows a schematic sectional view of the experimental configuration simulated (based on an experimental configuration commonly utilised at the University of Nottingham), which is a half cylinder-on-flat contact [19], while Fig. 1b is a two-dimensional schematic of the coating-substrate pair with an initial micro-crack. The corresponding 2D FE model is shown in Fig. 2. The general purpose, non-linear, commercial code ABAQUS (Version 6.8-1) is used throughout. The cylinder is modelled as a half circle with a radius of 6 mm and the flat is a rectangular shape of 12 × 6 mm in dimension. The coating is modelled as a perfectly adhered, single layer of thickness, t_c. The width of coating modelled is approximately twice that of the contact width, as shown schematically in Fig. 1a; comparative FE studies have established that the contact (surface and sub-surface) variable results in the coating regions are unaffected by this simplification [19]. This reduces the computational time of the simulations, particularly when combined with optimised mesh design.

Plane strain and linear quadrilateral elements were used. In order to improve the stress resolution with reasonable computational time, the mesh size was gradually refined towards the contact regions, as shown in Fig. 2b. In the coating region, the element size is equal to 20 μm at the coating edges and 1 μm at the crack seam. The transition from a coarse mesh (away from the contact regions) to a sufficiently refined mesh (in the contact regions) is achieved via the mesh control algorithm within ABAQUS. A mesh sensitivity study has been carried out on the effect of element size in the coating region on predicted crack length and shape. The element size is varied from 20 μm to 5 μm in the coating region (E_c = 100 GPa, E_s =200 GPa, t_c =500 μm, P = 500 N/mm, δ = 0.5 mm, μ = 0.3, K_{Ic} = 126 MPa.mm$^{1/2}$). The additional mesh refinement gives a negligible effect on predicted crack shape and length, but increases computational time from 4 hours to 60 hours.

Coulomb friction was employed, based on the Lagrange multiplier contact algorithm to ensure an exact sticking condition when the shear stress is less than the critical shear stress, according to Coulomb friction. A

range of coefficient of friction (COF) values between 0.3 and 0.7 are investigated for the contact surface; this range is typical for sliding contacts when one or both surfaces consist of a thermally sprayed coating [20 - 22]. The contact loading is simulated by applying a normal load, P, of 500 N/mm at a point on the top of the cylinder (Fig. 1a), based on previous experimental testing, e.g. see [19]. Unidirectional, tangential loading is applied incrementally via a tangential displacement, δ, of 0.1 mm at the same point (see Fig. 1a). Linear constraint equations were employed on the cylindrical top surface of the cylinder to ensure uniform horizontal and vertical displacement of nodes on the top surface. The bottom of flat (substrate) part is constrained in the x and y directions to prevent rigid body motion.

Attention is focussed in this paper on the regimes of linear elastic response of the materials. Two values of Young's modulus for the substrate, E_s, of 115 GPa and 200 GPa, are considered, to represent, respectively, the contrasting elastic properties of the widely-used lightweight alloy Ti-6Al-4V and high strength steels; in both cases, Poisson's ratio values of 0.3 are employed. These types of materials are commonly used for high performance contact applications where fretting and wear are important design considerations [23, 24]. The coating modulus, E_c values studied were 100 GPa and 200 GPa, as typical of thermally sprayed coating, e.g. see [25]. A value of 0.2 was assumed for Poisson's ratio of the coating [17]. Elastic mismatch of the coating is represented via the Dundur's first parameter, α for elastic moduli mismatch, and second parameter, β which includes the Poisson's ratio difference in addition to the elastic moduli [26]. The parameters are given by the following expression for a plane strain problem:

$$\alpha = \frac{\left(\frac{(1-\nu_s^{\,2})}{E_s} - \frac{(1-\nu_c^{\,2})}{E_c}\right)}{\left(\frac{(1-\nu_s^{\,2})}{E_s} + \frac{(1-\nu_c^{\,2})}{E_c}\right)} \tag{1}$$

$$\beta = \frac{1}{2}\left[\alpha - \frac{\left(\frac{\nu_s(1-\nu_s^{\,2})}{(1-\nu_s)E_s} - \frac{\nu_c(1-\nu_c^{\,2})}{(1-\nu_c)E_c}\right)}{\left(\frac{(1-\nu_s^{\,2})}{E_s} + \frac{(1-\nu_c^{\,2})}{E_c}\right)}\right] \tag{2}$$

where E and v are the elastic modulus and Poisson ratio respectively, with the subscripts s and c referring to the substrate and coating respectively. Values of α range from - 1 to + 1, where a negative value corresponds to a compliant coating bonded to a stiff substrate, and a positive value corresponds to a stiff coating on a compliant substrate. Value of α close to zero corresponds to situations where the coating and the substrate have similar compliance. The range of coating thickness studied, t_c, was from 100 to 200 μm, again, typical of thermally sprayed type coatings [25]. For simplicity, the residual stresses that normally occur in coatings due to the deposition process are not modelled.

Table 1 summarises the coating/substrate combinations investigated in the present work. The elastic mismatch between the coating and the substrate is represented by the Dundur's parameter, α, ranging from -0.356 to 0.245, the former value (α = -0.356) representing a compliant coating on stiff substrate and the latter value (α = 0.245) representing a stiff coating on a compliant substrate. The intermediate α values of -0.027 and -0.096 represent cases of relatively small elastic mismatch between the coating and the substrate. The ratio of coating thickness to contact semi-width (t/a_i) for all coating thickness models ranged between 0.38 and 1.03. This parameter is a measure of the influence of the coating on the overall contact stress distributions [8, 9]. The value of maximum contact pressure, P_{max} for each case is also presented in Table 1. For coatings with relatively small elastic mismatch (α values of -0.027 and -0.096), the predicted P_{max} value is close to the uncoated Hertzian value. In general, for compliant coatings, increasing thickness reduces P_{max} and increases contact semi width and vice versa for stiff coatings.

Figs. 3a to 3d show the subsurface tangential stress distributions for each case modelled under normal load, P and tangential displacement, δ if no pre-crack exist. All the stresses values are taken at 2.5 μm below the surface i.e. at the centroidal point of the first mesh layer below the surface at the end of horizontal displacement stroke. It can be seen that for the case of α values of -0.027 and -0.096 there is little changes in the maximum stress value with the change of thickness (Figs. 3c and d). For the case of α = -0.356 the maximum stress value is increasing with increasing thickness (Fig. 3b) and vice versa for the case of α = 0.245 (Fig. 3a).

Nodes on the coating of the cylindrical specimen were assigned as the master nodes and nodes on the coating of the flat specimen were assigned as the slave nodes. Contact interaction between the cylinder and the flat was defined using a finite sliding contact pair algorithm. The maximum allowable penetration depth (*h-crit*) between the slave and master nodes during the iterative solution process was defined as 0.2 μm. The minimum allowable distance between the initial coordinates of adjacent nodes on the mating contact surfaces (*ADJUST* parameter) was set to 0.002 μm.

Mesh validation of the contact model was conducted by comparison with the Hertzian solution [8] for a monolithic substrate. The FE model gave good agreement with the theoretical solution. The layered FE model was validated against the analytical solution presented in previous work [4, 10] for a cylindrical indenter on a layered substrate, for both contact pressure and interface stresses. To allow clear comparison between the published work and the results predicted by the current modelling technique, different coating thicknesses of 16, 40, 80, and 200 μm with E_c = 400 GPa, ν_c = 0.25 and E_s = 25 GPa, ν_s = 0.25 and a frictionless contact were modelled. The loading was kept at 50 N/mm for all the cases resulting in contact semi-width to coating thickness ratios (a_i/t_c) of 6.25, 1.8, 0.5 and 0.16 for coating thickness of 16, 40, 80, and 200 μm respectively; again within the range of solutions presented in the literature [4, 10]. Fig. 4a illustrates the pressure profiles for different contact semi-width to coating thickness ratios showing that the distributions deviate significantly from Hertzian behaviour for a significant elastic mismatch between the layer and the substrate as the layer thickness becomes relatively small compared to the contact semi-width, similar to the behaviour shown in the work of Gupta and Walowit [10]. For example, for a layer with a_i/t_c value of 0.5 (t_c = 80 μm) and y/a_i value of 0.8, the model predicted a p/p_o value of

0.6 which matches the corresponding value from [4, 10] to within 10%. As the layer thickness becomes relatively small compared to the contact semi-width, as for the case of a_i/t_c = 6.25 (t_c = 16 μm), there is a pressure peak of p/p_o ~ 0.95 at a horizontal position of y/a_i ~ 0.85 and a reduction of pressure to p/p_o ~ 0.87 at a horizontal position of y/a_i ~ 0.65. The same trend, in terms of location of pressure peak, and approximately the same peak pressure values are predicted by Gupta and Walowit [4, 10] for the case of a_i/t_c = 6. The stress distributions, taken at the centroidal points of the FE elements (a distance of 2 μm from the interface) for the case of a coating thickness of 40 μm (a_i/t_c = 1.8), are shown in Fig. 4b; the FE model results are similar to the contact solutions presented in the literature [4, 10, 19].

2.2. Crack growth model

A crack growth model for unstable crack growth in the coating has been developed, based on linear elastic fracture mechanics (LEFM) analysis of the crack tip. The model has been developed using the Python programming language to automatically update the crack geometry to account for unstable crack growth under a quasi-static conditions, based on the FE-predicted evolution of the crack tip stress intensity factor.

An *a priori* crack of length *c* is inserted into the surface of the coated flat specimen at the trailing edge of the contact, the selection of location being made in light of the high tensile stress in this position as it slides [5, 14 and 15], as shown schematically in Fig. 1b. The initial crack is modelled as an embedded line called a 'seam' in ABAQUS. A seam defines an edge or face in the model that is originally closed but can open during an analysis. Overlapping duplicate nodes are placed along a seam when the mesh is generated. These coincident nodes are free to move apart as the seam separates. The crack faces are assumed not to come in contact with each other and therefore crack face friction is not modelled here. In this work, a seam is modelled from the surface inwards perpendicular to the free surface. The corresponding length of the seam is equivalent to the pre-existing microcrack of 10 μm. This corresponds to a crack to contact semi width ratio, c/a_i, of approximately 0.05. This value is sufficient to give the highest stress intensity factor in the system for the crack located at the contact edge [14, 15]. The crack tip is defined at a node located at the end of the crack seam. A sweep plane strain quadrilateral mesh is used for the contour integral analysis. A series of five rings of quadrilateral elements are assigned along the crack seam, centred on the crack tip, as shown in Fig. 5a, and the radial dimension of the elements along the seam is reduced closer to the crack tip to provide accurate crack tip resolution of displacements, strains and stresses for the contour integral analysis. The meshes are also refined around the crack path to increase accuracy (Figs. 5b and 2b).

The criterion for unstable crack propagation is that of the stress intensity factor (SIF) exceeding the fracture toughness $K_I > K_{IC}$ [15, 16] as implemented within the ABAQUS/Python code interaction. The fracture toughness of the coating ranges from 80 to 100 MPa.mm$^{1/2}$ (2.53 to 3.16 MPa.m$^{1/2}$), these values being typical for thermally sprayed coatings, e.g. see [25]. For the initial crack, the crack propagation direction is set to be parallel to the crack seam and inwards from the surface. The subsequent crack propagation direction, i.e., the angle at which a pre-existing crack will propagate, θ is determined by the contour integral analysis of stress intensity factor around

the crack tip by ABAQUS based on the criterion of the mode II stress intensity factor being equal to zero ($K_{II} = 0$). This can be justified in light of the work of Oliveira and Bower [16] in their study of fracture and delamination of thin coatings under contact loading where they demonstrated that K_{II} has little effect on the final mixed-mode fracture path. Furthermore, it is shown by Cotterell and Rice [27] and stated in ABAQUS theory manual [28] that the crack propagation for zero K_{II} ($K_{II} = 0$) has little different on other crack propagation direction criterion such as maximum tangential stress criterion and maximum energy release rate criterion. This angle at which a pre-existing crack will propagate is measured counter-clockwise from the initially defined crack extension direction. It is important to note that during the application of tangential displacement, the amount of displacement is applied incrementally, thus in some cases the crack will propagates even when the tangential load is less than sliding force μP.

The crack propagation is controlled using an assumed crack length increment, dc. A value of dc of 5 μm is found here to give a converged solution. The combined frictional contact and crack propagation simulation tool operates as shown in the flowchart of Fig. 6. Starting with the initial crack length, and for every subsequent crack length and shape, a frictional contact analysis, incorporating normal and tangential loading, is performed, to evaluate the crack tip K_I to evaluate whether or not the evolving crack should be extended by another increment. As the displacement is applied incrementally, the crack tip K_I is calculated and its corresponding plane, θ is recorded, based on the criterion of $K_{II} = 0$. ABAQUS will obtain a pair of K_I and θ values for every increment and passes it to the Python code. Once the crack tip K_I has exceeded the fracture toughness ($K_I > K_{IC}$) of the coating, the corresponding plane, θ of the crack tip K_I is taken as the crack propagation angle. This is continued until the crack arrests, i.e. crack propagation ceases, either due to $K_I < K_{IC}$ or proximity to the substrate-coating interface. For $K_I > K_{IC}$, the Python program creates a new model by extending the crack seam for a length of dc at an angle θ, corresponding to the crack propagation direction from the previous analysis. Fig. 5b shows representative crack propagation from the analysis. The present code is not designed to deal with interface delamination and therefore cracks can only propagate to within a small distance (5 μm, viz. contour integral mesh size) of the substrate-coating interface.

3. Results

3.1. Effect of elastic mismatch and coating thickness

Figs. 7a, 7b and 7c show the predicted crack trajectories for different thickness of coating, across the range of α values indicated in Table 1. Referring to Fig. 7a, for the thinnest coating, crack propagation was predicted for three coating-substrate combinations, but only the stiff coating cases propagated close to the interface. Referring to Fig. 7c, the thickest coating, only the steel substrate cases were predicted to give propagation and, in these cases, propagation was only predicted to half coating thickness. The same is true for the intermediate coating

thickness (Fig. 7b), but the stiffer coating in this case is predicted to propagate to a longer length. The stiffest coating with largest mismatch (α = 0.245) was not predicted to give propagation for the thickest or intermediate coating thickness cases. The stiffer coatings gave greater deviation of crack direction from perpendicular. These results suggest that crack propagation in coatings with greater elastic mismatch is more sensitive to changes of coating thickness.

3.2. Effect of coefficient of friction

Figs. 8 and 9 show the effect of COF on the predicted crack propagation for α values of 0.245 (stiff coating) and -0.356 (compliant coating) for 100 and 200 μm thick coatings respectively. For the stiff 100 μm coating (Fig. 8a), the COF is predicted to have a negligible effect on crack length and only a small effect on the crack direction, causing it to grow closer to the direction perpendicular to the surface; for the compliant 100 μm coating (Fig. 8b), the increase in COF again has a negligible predicted effect on crack direction but is predicted to affect the length significantly, with the crack length doubling as the COF increases from 0.3 to 0.5, leading to a through-thickness coating crack. The predicted effect of changes in COF is similar for α values of -0.356 (compliant coating) for the 200 μm thick coating, with the higher COF value leading to through-thickness coating cracks for coating compliant (Fig. 9b). For an α value of 0.245 (stiff coating) with 200 μm thickness, the crack is not predicted to propagate for a COF of 0.3; increasing the COF to 0.5 results in a through-thickness coating crack (Fig. 9a). These results are consistent with the K_I value of the crack increasing with increasing COF, due to higher trailing edge tensile stresses for example.

Figs. 10a and 10b show the effect of COF on the subsurface (2.5 μm below the surface) tangential stress distributions for the case of α = 0.245 and α = -0.356 under normal load, P and tangential displacement, δ with no pre-crack exist. In general, the maximum stress value at the trailing edge of contact is increasing with increasing COF. It also can be seen that the case of α = 0.245 (E_c200/Ti-6Al-4V) is having slightly higher maximum stress values compare to the case of α = -0.356 (E_c100/steel) for COF 0f 0.5..

3.3. Effect of coating fracture toughness

The effect of the coating fracture toughness, K_{IC}, on the steady state propagated crack profile is shown in Fig. 11 for a compliant (α = -0.356) 200 μm thick coating. The predicted crack profiles vary in a complex manner with increasing K_{IC} value; as the toughness increases, the final crack length decreases, but the final path of the crack also deviates towards the contact. In general the overall effect of fracture toughness within the range considered is not significant.

3.4. The evolution of K_I stress intensity

In order to further understand the interaction between the contact conditions and fracture mechanics for coated specimens, the effect of applied tangential displacement (stroke) on the mode I SIF, K_I of the final propagated crack (viz. on the resulting final cracks shown in Fig. 7) is predicted. The results are plotted in Fig. 12 for the analyses of Table 1.

Fig. 12a shows in greater detail the predicted effect of tangential displacement on the evolution of K_I for a stiff coating (α = 0.245). It is clear that coating thickness has a more significant effect than for less mismatched coatings, viz. Figs. 12c and 12d. Crack propagation is only predicted for the thin coating in Fig. 12a. These results, along with those of Fig. 7, indicate that for a stiff coating, increased coating thickness is beneficial to cracking resistance.

The results of Fig. 12b, (also consistent with the results of Fig. 7), suggest, that for a compliant coating (α = -0.356), increasing thickness will increase the final crack length, albeit only to half coating depth. This is due to the higher K_I value reached at the end of horizontal displacement stroke. However, as shown in Fig. 9, increasing COF can lead to through-thickness cracking even for the same amount of applied displacement.

Figs. 12c and 12d show the predicted effect of coating thickness on SIF-displacement response for low mismatch coatings (α = -0.096 and α = -0.027). In both cases, coating thickness is predicted to have a negligible effect on the response. The system with α = -0.027, which is the system with the highest degree of matched stiffness, generally exhibits lower SIF values than all other coatings considered here. However, with increasing tangential displacement to 100 μm, the critical SIF value is reached so that propagation does occur for all coating thickness values.

4. Discussion

The results presented in the present work are in accord with previous stress analyses of layered (uncracked) contact under normal and tangential loading [12, 13, 19], which showed that the tensile stress at the trailing edge of the contact (and the associated brittle fracture of the coating) decreases with increasing thickness for a stiff coating on a complaint substrate (i.e. $\alpha > 0$) and vice versa for a compliant coating on stiff substrate (i.e. $\alpha < 0$). It is also shown that for small elastic coating-substrate mismatches, the stress is less sensitive to coating thickness.

With regard to the results presented here, it is predicted that the initial microcrack does not propagate with increasing thickness for an α value of 0.245 (Fig. 7a), while for the α value of -0.356, the propagated crack increases in length with increasing thickness (Fig. 7). For an α value of -0.027 (small elastic mismatch), the final crack length is relatively insensitive to coating thickness. This is consistent with the predicted tangential stress distributions as shown in Fig. 3. For a compliant coating, as the coating thickness increases, the maximum tangential stress at the trailing edge increases, thus the tendency for crack propagation increases (Fig. 3b). Furthermore, it is also shown that for a case of high elastic mismatch, the tangential stress predicted is more sensitive to the change of coating thickness (Figs. 3a and 3b). For example, for the case of α = 0.245, the cracks

only propagate for a 100 μm thick coating (Table 1 and Fig. 7a), due to the reduction of tangential stress with increasing thickness (Fig. 3a). However, for the case of α = -0.356, the crack length increases with increasing thickness (Table 1 and Figs. 7), consistent with the predicted tangential stress distribution (Fig. 3b). This evidence can be further seen from the plot of stress intensity factor evolution with increasing displacement (for the final propagated crack) as shown in Fig. 12a and 12b for α values of 0.245 and -0.356. The effect on stress intensity factor for each case with the changes of thickness (Fig. 12) is also consistent with the predicted tangential stress distribution (Fig. 3).

Gupta and Walowit [4] found that the maximum tangential stress for a relatively stiff coating reduces with increase in coating thickness and that the stresses were a few magnitude higher than the applied stress for a stiff, thin coating. Djabella and Arnell [12] however showed that increasing coating stiffness does not necessarily increase trailing edge tangential stress in the coating for relatively stiff coatings. Depending on the COF and the relative thickness of the coating to the contact semi-width, the maximum tangential stress may reduce with increasing coating stiffness.

For the case of a stiff coating ($\alpha > 0$), a region of tensile stress is predicted at the coating-substrate interface, below the centre of contact, due to the effect of normal load. Similar behaviour has also been reported by [16]. For the case of Ec200/Ti-6Al-4V (α = 0.245) the size of the tensile region at the coating-substrate interface increases with increasing coating thickness. The value of the stress however is much lower than the (sliding) trailing edge tensile stress experienced. The trailing edge value increases further with increasing COF.

Fig. 8a shows a small effect on final crack length and direction due to increasing COF from 0.3 to 0.5. This case corresponds to a stiff, thin coating (α = 0.245 and 100 μm thick). In this case, the high stress region is concentrated within the coating and, although increasing COF will increase the stresses (Fig. 10), even for a COF of 0.3, the crack propagates to the interface, i.e. $K_I > K_{IC}$. In contrast, for the compliant coating of Fig. 8b (α = -0.356), the stresses are less concentrated in the coating and the crack does not propagate to the interface for COF of 0.3; however, in this case, increasing the COF to 0.5 increases the stress levels and the degree of concentration of stresses near the surface (in the coating), thus leading to propagation to the interface.

The deviation of the propagated crack away from the contact region for $\alpha > 0$ is due to the high compressive stress experience by the coating close to the interface. Since the coating is stiffer than the substrate, the coating fulfils a load bearing role under normal load thus higher compressive stresses in this region are developed. Similar results have been presented in earlier work [12, 29], which showed that the compressive stress at the coating/substrate interface trailing edge is higher for stiffer coatings. With increasing COF, the tensile stress will increase, thus reducing the crack deviation (Figs. 8 and 9). This behaviour has also been reported in earlier work [12, 16].

The results of Fig. 11 for a compliant (α = -0.356) 200 μm thick coating shows that the coating fracture toughness, K_{IC}, affects the final crack pattern of the coating. For a different K_{IC} value with the same COF and thickness, crack propagation will occur at different points in the tangential loading cycle. This will directly alter

the stresses around the crack tip and consequently lead to different predicted subsequent crack growth, including direction (path).

Fig. 13 shows the result of an additional analysis for a 500 μm thick compliant (α = -0.356) coating, with an applied displacement of 0.5 mm and a fracture toughness of 126 MPa.mm$^{1/2}$ (measured value for a WC-Co HVOF thermally sprayed coating from [25]), for different assumed COF values of 0.3, 0.5 and 0.7. The propagated cracks increase in length with increasing COF and for the highest COF of 0.7, the final predicted crack profile grows under the contact, moving away from the coating/substrate interface. These COF trends are in excellent agreement with those of earlier research [15, 16, 30], which has in turn been validated by experimental results. This phenomenon is attributed to the large t_c/a_i ratio ($t_c/a_i \sim 2$) and the influence of the stiff substrate.

The predicted dependency of K_I on tangential displacement (distance of load from crack), as shown in Fig. 12, is controlled by a complex interaction between (i) stress distributions in the coating, (ii) the current position of the crack tip and (iii) the current displacement. In some cases, the crack tip deflects towards the underside of the contact and in other cases it deflects away from the underside of the contact. The variation of K_I with distance from load is consistent with that presented by Oliveira and Bower [16]

The current work assumes homogeneous fracture toughness throughout the coating thickness. However, it has been reported [25, 31] that regions of lower fracture toughness might exist within the coating due to microstructural inhomogeneities in thermally sprayed coatings (associated with their spalt-like build-up). It should also be noted that the methodology presented is only applicable to materials susceptible to brittle, fast (unstable) fracture behaviour, as opposed to situations where fatigue (stable) crack growth dominates [32].

5. Conclusions

The current work illustrates the effectiveness of FE analysis as a tool to simulate the fast fracture behaviour in a layered substrate subjected to normal and tangential loading. A Python code for automated FE modelling of crack propagation has been developed to predict the fast fracture of brittle coatings under normal and tangential loading. This makes it possible to study the effects of various coating parameters in isolation. The present work focussed on the effect of elastic mismatch, coating thickness, coefficient of friction and coating fracture toughness on crack propagation. The predictions lead to the following conclusions:

- The propagation of cracks for coating-substrate systems with large elastic mismatch, i.e. large α values (e.g. α = 0.245, -0.356), is found to be sensitive to changes in coating thickness.
- The risk of crack propagation is increased (i) with increasing coating thickness for compliant coatings, negative α values, (e.g. α = -0.356) and (ii) with decreasing coating thickness for stiff coatings, positive α values (e.g. α = 0.245).
- The effect of changing coating thickness on the final propagated crack is less significant for a coating which has similar stiffness to the substrate (e.g. α = -0.027, -0.096).

- Reduction in the α value (making the system more matched) is predicted to reduce the crack deviation away from the contact region.
- Increasing the contact coefficient of friction will increase the propagated crack length and reduce the crack deviation (i.e. make cracks more perpendicular to the surface).
- The predicted crack profiles vary in a complex way with changes in the fracture toughness of the coating.
- The final crack profiles are predicted to deflect parallel to the interface towards the underside of the contact for thick coatings ($t_c/a_i \sim 2$) with large applied sliding displacement ($\delta/a_i = 2$).

Acknowledgements

This research was carried out at the University Technology Centre in Gas Turbine Transmission Systems at the University of Nottingham with financial support from Rolls-Royce plc, Aerospace Group. The views expressed in this paper are those of the authors and not necessarily those of Rolls-Royce plc, Aerospace Group.

References

[1] A. Leyland, A. Matthews, On the significance of the H/E ratio in wear control: a nanocomposite coating approach to optimised tribological behaviour. Wear 246 (2000) 1-11.

[2] Q. Wei, J. Narayan, Superhard diamondlike carbon: preparation, theory, and properties. Int. Mater. Rev. 45 (2000) 133-164.

[3] S.J. Bull, E.G. Berasetegui, An overview of the potential of quantitative coating adhesion measurement by scratch testing. Tribology International 39 (2006) 99-114.

[4] P.K. Gupta, J.A. Walowit, E.F. Finkin, Stress distributions in plane strain layered elastic solids subjected to arbitrary boundary loading. Journal of Lubrication Technology-Transactions of the ASME 95 (1973) 427-433.

[5] K. Holmberg, A. Laukkanen, H. Ronkainen, K. Wallin, Tribological analysis of fracture conditions in thin surface coatings by 3D FEM modelling and stress simulations. Tribology International 38 (2005) 1035-1049.

[6] A. Strawbridge, H.E. Evans, Mechanical failure of thin brittle coatings. Eng. Fail. Anal. 2 (1995) 85-103.

[7] M. Shima, J. Okado, I.R. McColl, R.B. Waterhouse, T. Hasegawa, M. Kasaya, The influence of substrate material and hardness on the fretting behaviour of TiN. Wear 225-229 (1999) 38-45.

[8] K.L. Johnson, Contact Mechanics, Cambridge University Press, Cambridge, 1985.

[9] P. Meijers, The contact Problem of a Rigid Cylinder on an Elastic Layer, Applied Scientific Research, 18 (1968), 353.

[10] P.K. Gupta, J.A. Walowit, Contact stresses between an elastic cylinder and a layered elastic solid. Journal of Lubrication Technology-Transactions of the ASME 96 (1974) 250-257.

[11] S.J. Cole, R.S. Sayles, A numerical-model for the contact of layered elastic bodies with real rough surfaces. Journal of Tribology-Transactions of the ASME 114 (1992) 334-340.

[12] H. Djabella, R.D. Arnell, Finite-element analysis of the contact stresses in elastic coating substrate under normal and tangential load. Thin Solid Films 223 (1993) 87-97.

[13] H.H. Bennani, J. Takadoum, Finite element model of elastic stresses in thin coatings submitted to applied forces. Surface and Coatings Technology 111 (1999) 80-85.

[14] D. A. Hills, R L Munisamy, D Nowell, A G Atkins, Brittle fracture from a sliding hertzian contact. Proceedings of the Institution of Mechanical Engineers, Part C: Journal of Mechanical Engineering Science 208 (1994) 409-415.

[15] A.F. Bower, N.A. Fleck, Brittle fracture under a sliding line contact. Journal of the Mechanics and Physics of Solids 42 (1994) 1375-1396.

[16] S.A.G. Oliveira, A.F. Bower, An analysis of fracture and delamination in thin coatings subjected to contact loading. Wear 198 (1996) 15-32.

[17] D. Dalmas, S. Benmedhakene, H. Kebir, C. Richard, A. Laksimi, J.M. Roleandt, Investigation of failure mechanisms in WC-Co coated materials. Surf. Coat. Technol. 173 (2003) 130-143.

[18] P. Bansal, P.H. Shipway, S.B. Leen, Finite element modelling of the fracture behaviour of brittle coatings. Surface and Coatings Technology 200 (2006) 5318-5327.

[19] A.L. Mohd Tobi, J. Ding, S. Pearson, S.B. Leen, P.H. Shipway, The effect of gross sliding fretting wear on stress distributions in thin W-DLC coating systems. Tribology International 43 (2010) 1917-1932.

[20] Y.-c. Zhu, K. Yukimura, C.-x. Ding, P.-y. Zhang, Tribological properties of nanostructured and conventional WC-Co coatings deposited by plasma spraying. Thin Solid Films 388 (2001) 277-282.

[21] K. Kubiak, S. Fouvry, A.M. Marechal, J.M. Vernet, Behaviour of shot peening combined with WC-Co HVOF coating under complex fretting wear and fretting fatigue loading conditions. Surface and Coatings Technology 201 (2006) 4323-4328.

[22] K. Bonny, P. De Baets, Y. Perez, J. Vleugels, B. Lauwers, Friction and wear characteristics of WC-Co cemented carbides in dry reciprocating sliding contact. Wear 268 (2010) 1504-1517.

[23] S.B. Leen, I.J. Richardson, I.R. McColl, E.J. Williams, T.R. Hyde, Macroscopic fretting variables in a splined coupling under combined torque and axial load. Journal of Strain Analysis for Engineering Design 36 (2001) 481-497.

[24] J.J. Madge, S.B. Leen, I.R. McColl, P.H. Shipway, Contact-evolution based prediction of fretting fatigue life: Effect of slip amplitude. Wear 262 (2007) 1159-1170.

[25] L.C. Driver, HVOF Spraying of WC-Co & MCrAlY Coatings for Aeroengine Components, PhD thesis. University of Nottingham, 2004.

[26] J. Dundurs, Discussion of edge-bonded dissimilar orthogonal elastic wedges under normal and shear loading. Journal of Applied Mechanics 36 (1969), 650–652.

[27] B. Cotterell, J. R. Rice, Slightly Curved or Kinked Cracks. International Journal of Fracture 16 (1980), 155–169.

[28] Abaqus Theory Manual.Version 6.10. RI, USA: Dassault Systèmes; 2010.

[29] K. Holmberg, H. Ronkainen, A. Laukkanen, K. Wallin, A. Erdemir, O. Eryilmaz, Tribological analysis of TiN and DLC coated contacts by 3D FEM modelling and stress simulation. Wear 264 (2008) 877-884.

[30] B. Chiaia, Fracture mechanisms induced in a brittle material by a hard cutting indenter. Int. J. Solids Struct. 38 (2001) 7747-7768.

[31] T. Sudaprasert, An investigation of microstructure and sliding wear in thermally sprayed WC-Co coatings, PhD thesis. University of Nottingham, 2002.

[32] D. Dini, D. Nowell, I.N. Dyson, The use of notch and short crack approaches to fretting fatigue threshold prediction: Theory and experimental validation. Tribology International 39 (2006) 1158-1165.

Figure(s)

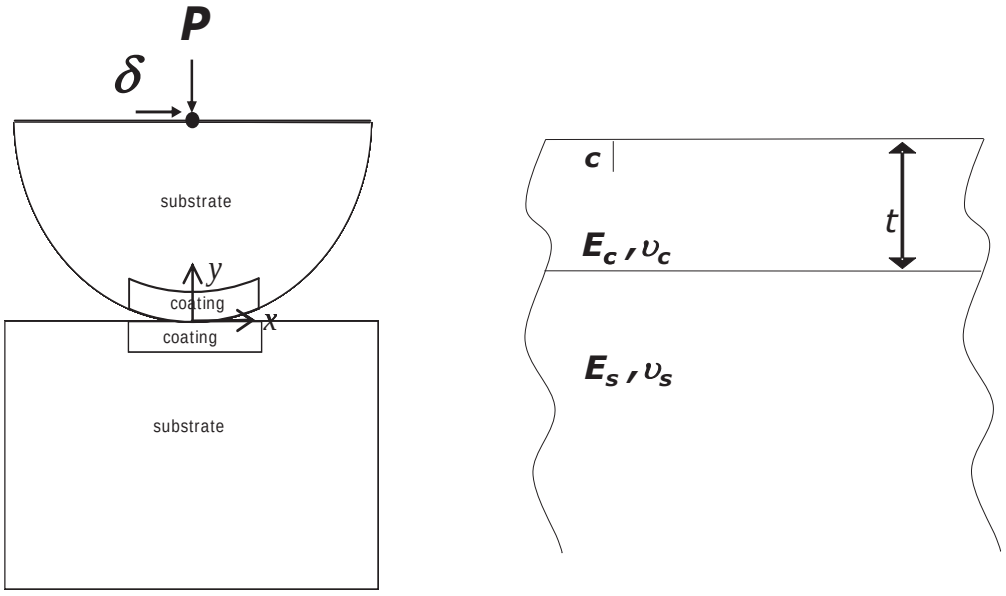

(a) (b)

Fig. 1. (a) Schematic view of the half cylinder-on-flat coated substrate model and (b) schematic view of the initial microcrack within the coating on the flat specimen.

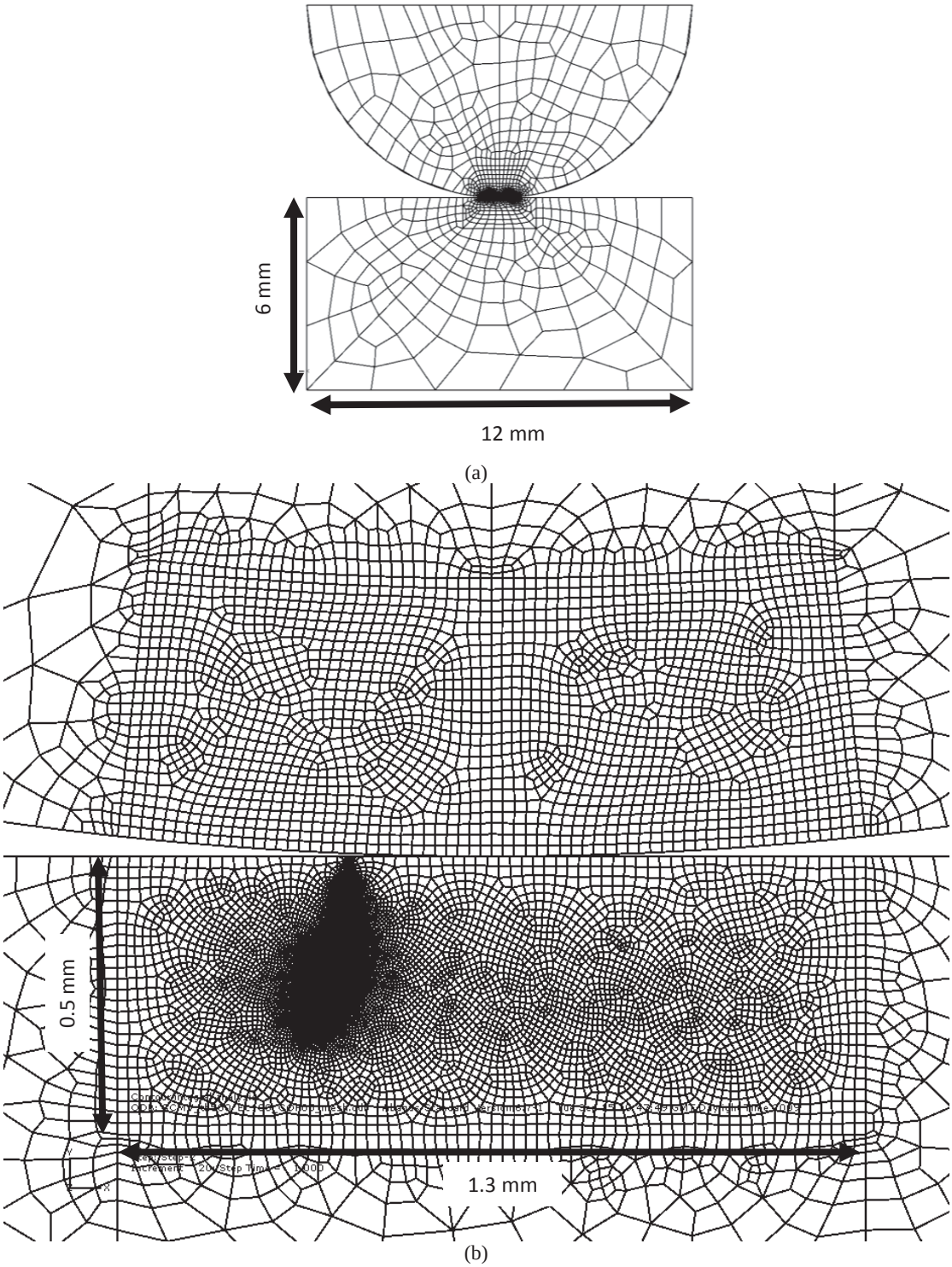

Fig. 2. (a) Finite element full model mesh and (b) contact region mesh detail showing fine mesh around the crack profile.

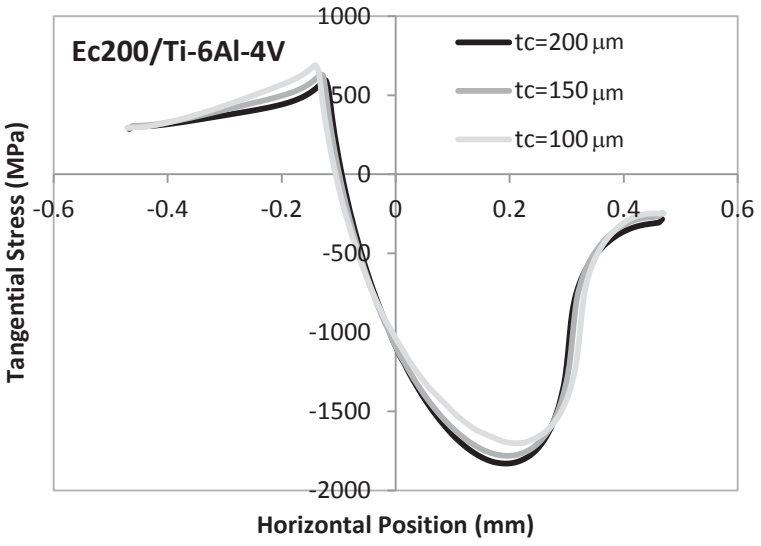

(a)

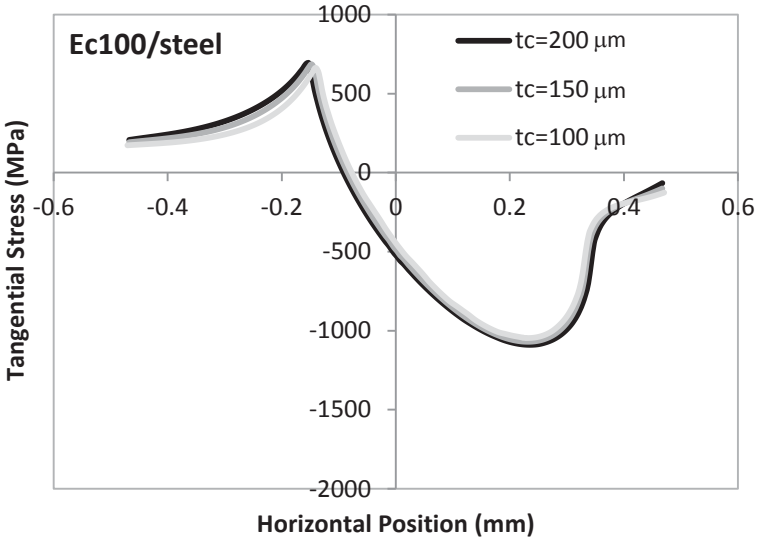

(b)

Fig. 3. FE predicted tangential stress distributions (taken at 2.5 μm below the surface) for the case of (a) α = 0.245, (b) α = -0.356, (c) α = -0.096 and (d) α = -0.027 for no pre-crack model at the end of contact sliding. (P = 500 N/mm, δ = 0.1 mm, μ = 0.3).

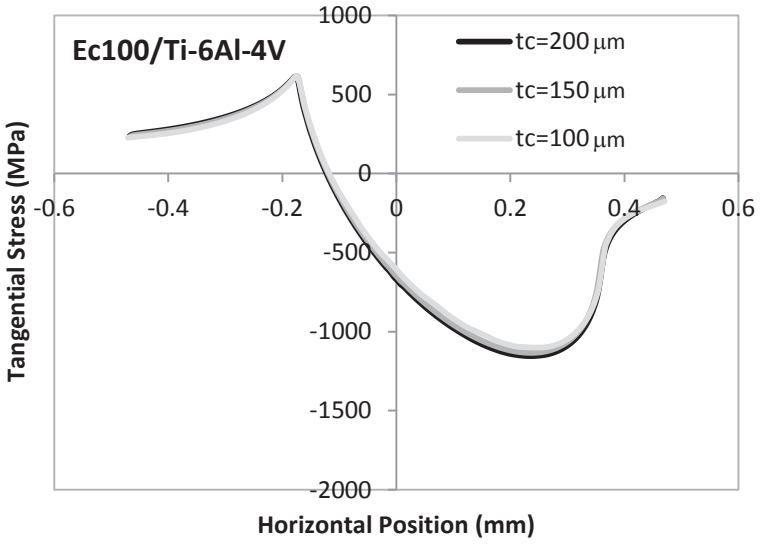

(c)

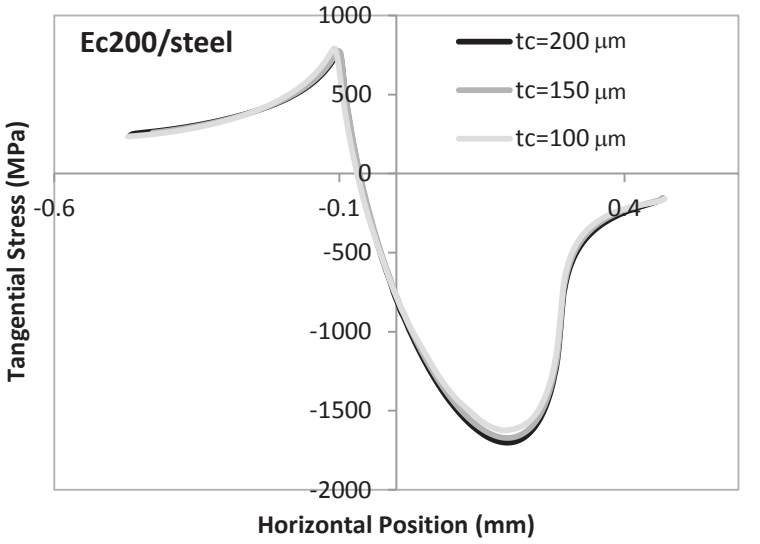

(d)

Cont. Fig. 3. FE predicted tangential stress distributions (taken at 2.5 μm below the surface) for the case of (a) $\alpha = 0.245$, (b) $\alpha = -0.356$, (c) $\alpha = -0.096$ and (d) $\alpha = -0.027$ for no pre-crack model at the end of contact sliding. (P = 500 N/mm, δ = 0.1 mm, μ = 0.3).

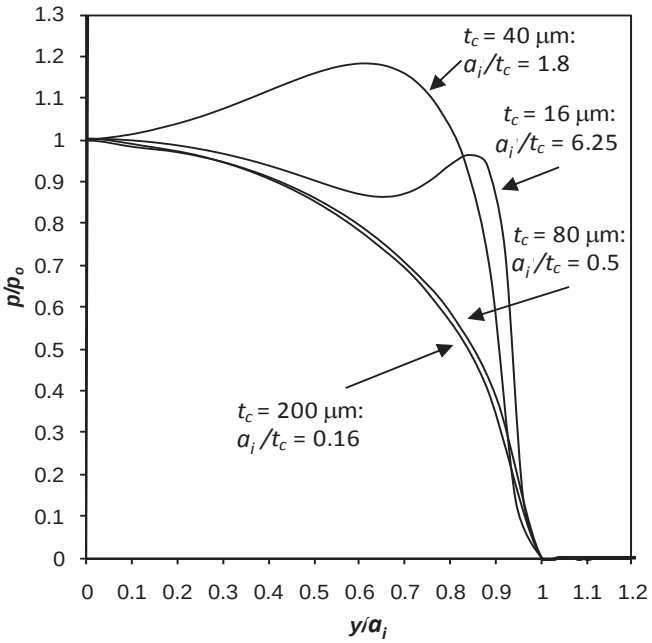

(a)

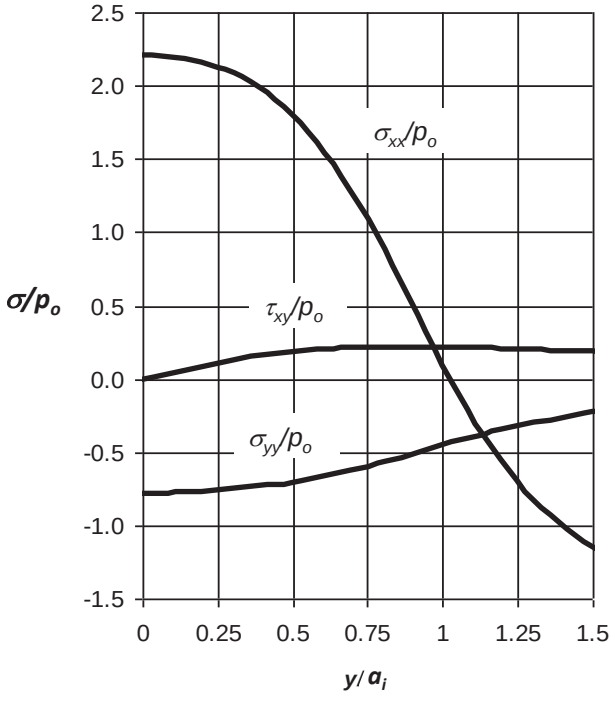

(b)

Fig. 4. FE predicted (a) contact pressure distributions, p of rigid cylinder (6 mm radius) on layered substrate relative to its central pressure, p_o for different contact semi width to layer thickness ratio, a_i/t_c, (b) stress distributions at the coating interface for the case of a_i/t_c = 1.8 (t_c = 40 μm) (after [5, 10]): (P = 50 N/mm, E_c = 400 GPa, E_s = 25 GPa, $\nu_c = \nu_s$ = 0.25, μ = 0).

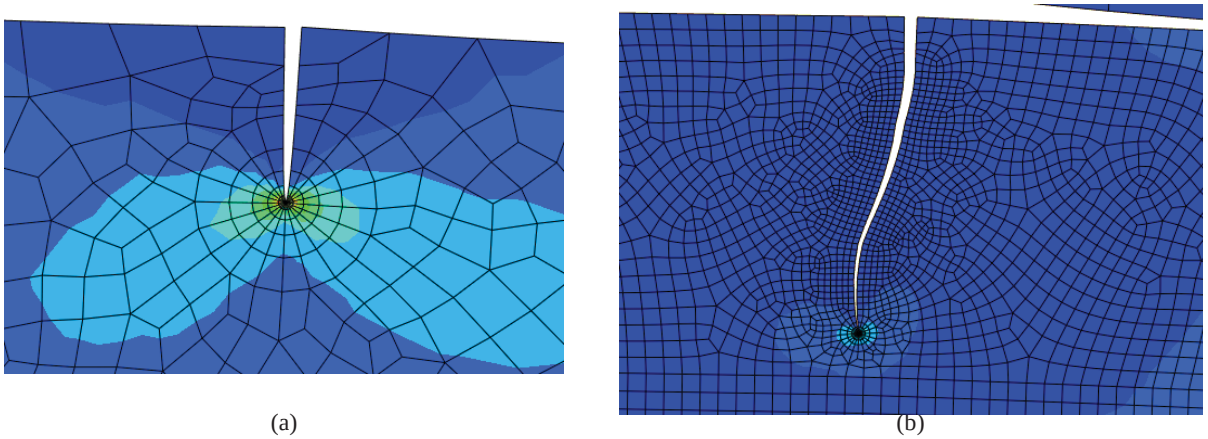

(a) (b)

Fig. 5. FE model results showing (a) the initial 10 μm crack at the contact trailing edge, (b) the steady state profile of a crack propagated from the initial 10 μm flaw.

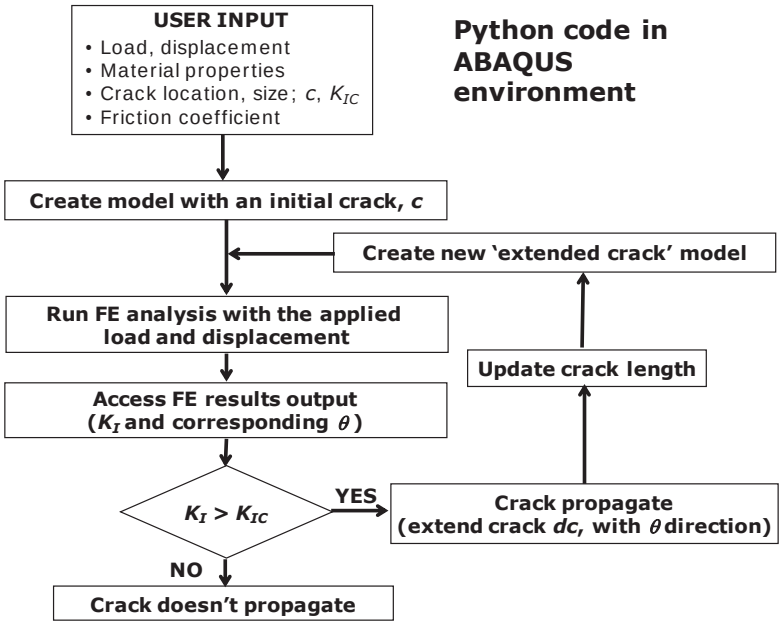

Fig. 6. Flowchart illustrating coating crack growth algorithm implemented in Python code for FE-based fast fracture model in ABAQUS.

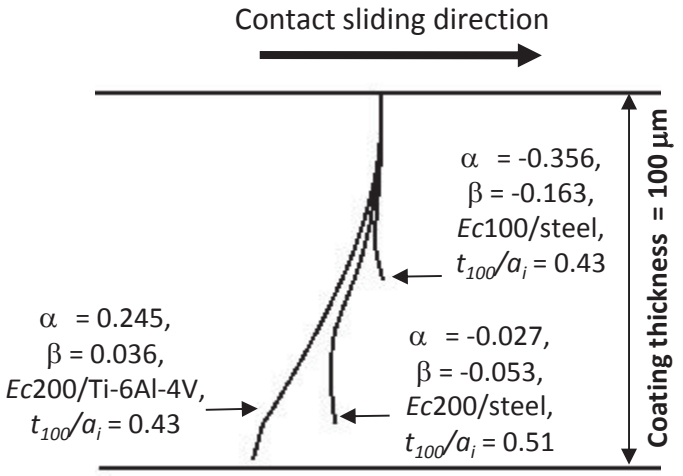

(a)

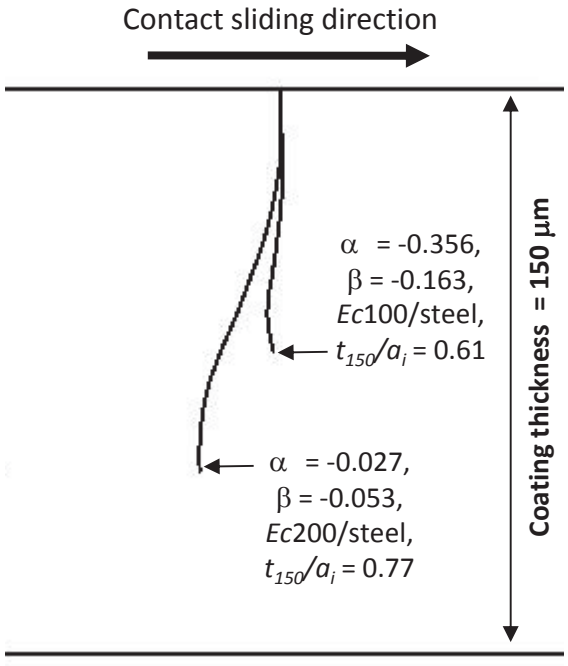

(b)

Fig. 7. Predicted effect of coating thickness on coating crack propagation for (a) 100 µm, (b) 150 µm and (c) 200 µm thick coatings, for α values of 0.245, -0.027 and -0.356 (P = 500 N/mm, δ = 0.1 mm, μ = 0.3, K_{IC} = 100 MPa.mm$^{1/2}$), (Same scale is applied on vertical and horizontal axis).

.

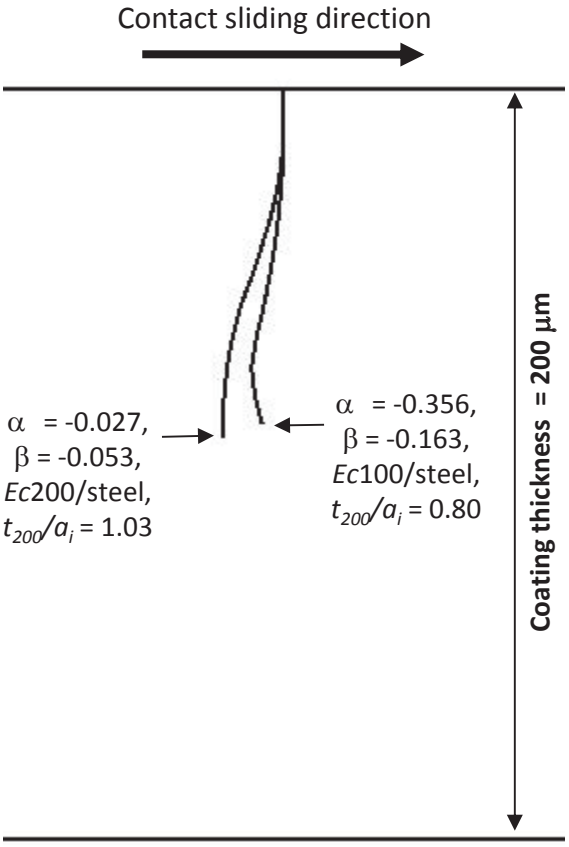

(c)

Cont. Fig. 7. Predicted effect of coating thickness on coating crack propagation for (a) 100 μm, (b) 150 μm and (c) 200 μm thick coatings, for α values of 0.245, -0.027 and -0.356 (P = 500 N/mm, δ = 0.1 mm, μ = 0.3, K_{IC} = 100 MPa.mm$^{1/2}$), (Same scale is applied on vertical and horizontal axis).

.

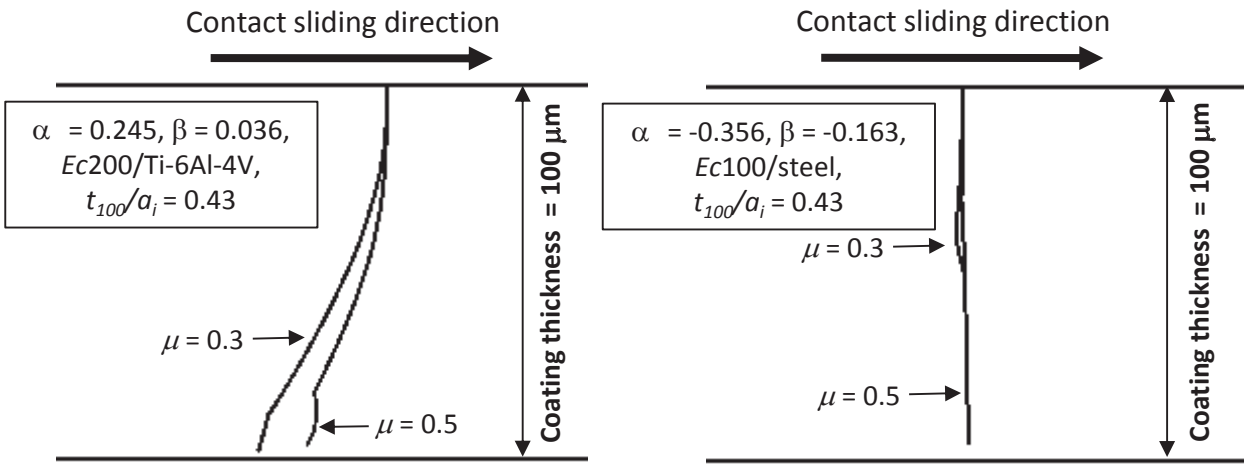

(a) (b)

Fig. 8. Predicted effect of COF on coating crack propagation in 100 μm thick coating for α values of (a) 0.245, and (b) -0.356 (P = 500 N/mm, δ = 0.1 mm, K_{IC} = 100 MPa.mm$^{1/2}$), (Same scale is applied on vertical and horizontal axis).

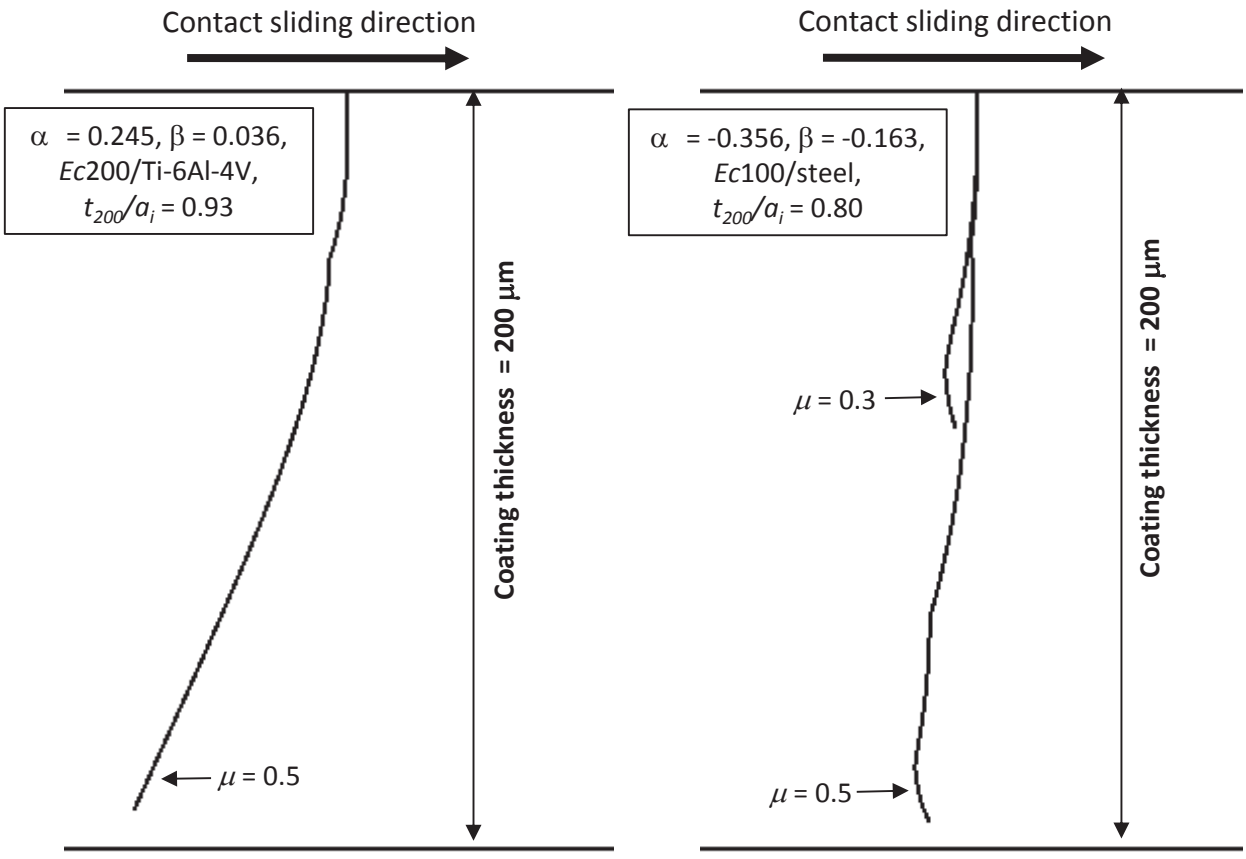

(a) (b)

Fig. 9. Predicted effect of COF on coating crack propagation in 200 μm thick coating for α values of (a) 0.245, and (b) -0.356 (P = 500 N/mm, δ = 0.1 mm, K_{IC} = 100 MPa.mm$^{1/2}$), (Same scale is applied on vertical and horizontal axis).

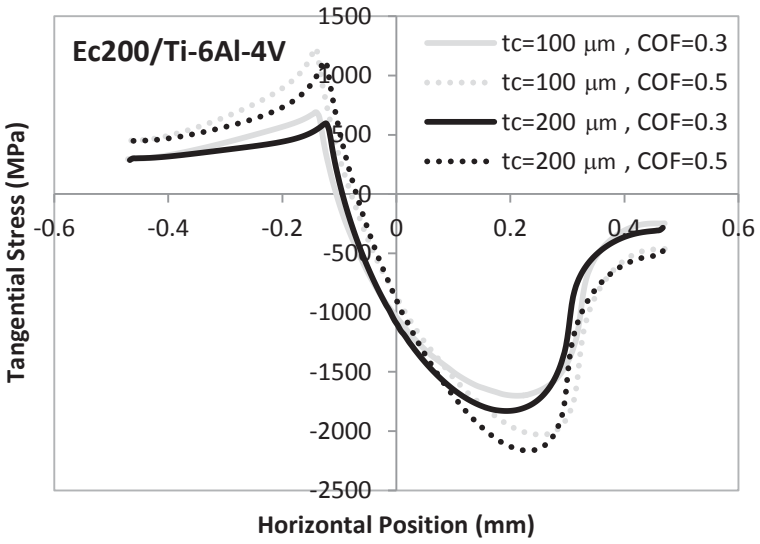

(a)

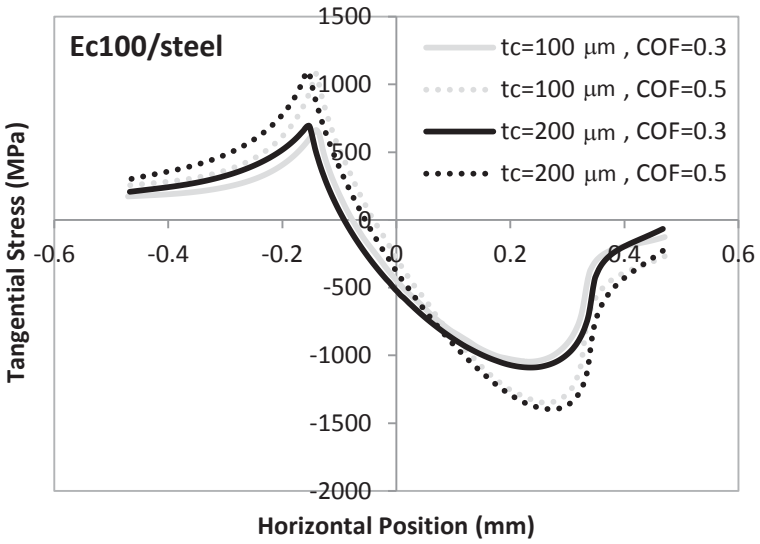

(b)

Fig. 10. FE predicted tangential stress distributions (taken at 2.5 μm below the surface) for the case of (a) $\alpha = 0.245$ and (b) $\alpha = -0.356$ for no pre-crack model at the end of contact sliding. (P = 500 N/mm, δ = 0.1 mm, t_c = 100 and 200 μm).

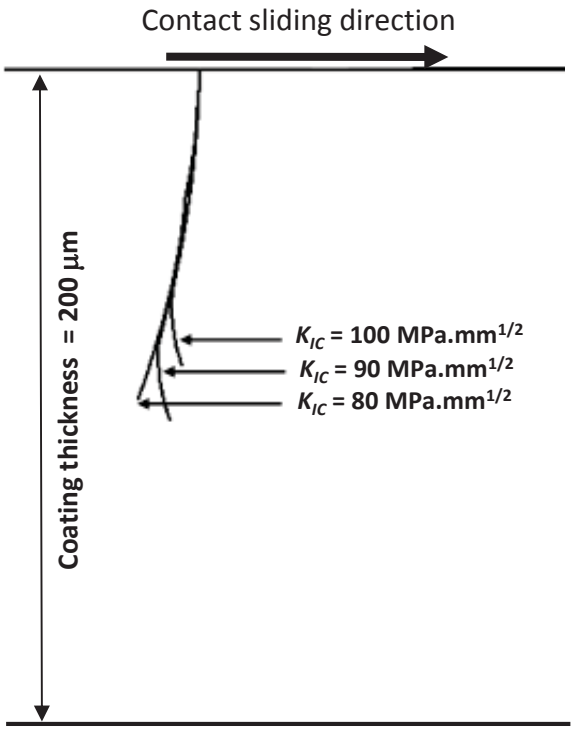

Fig. 11. Predicted effect of coating fracture toughness on crack profiles (α = -0.356, t_c = 200 μm, P = 500 N/mm, δ = 0.1 mm, μ = 0.3), (Same scale is applied on vertical and horizontal axis).

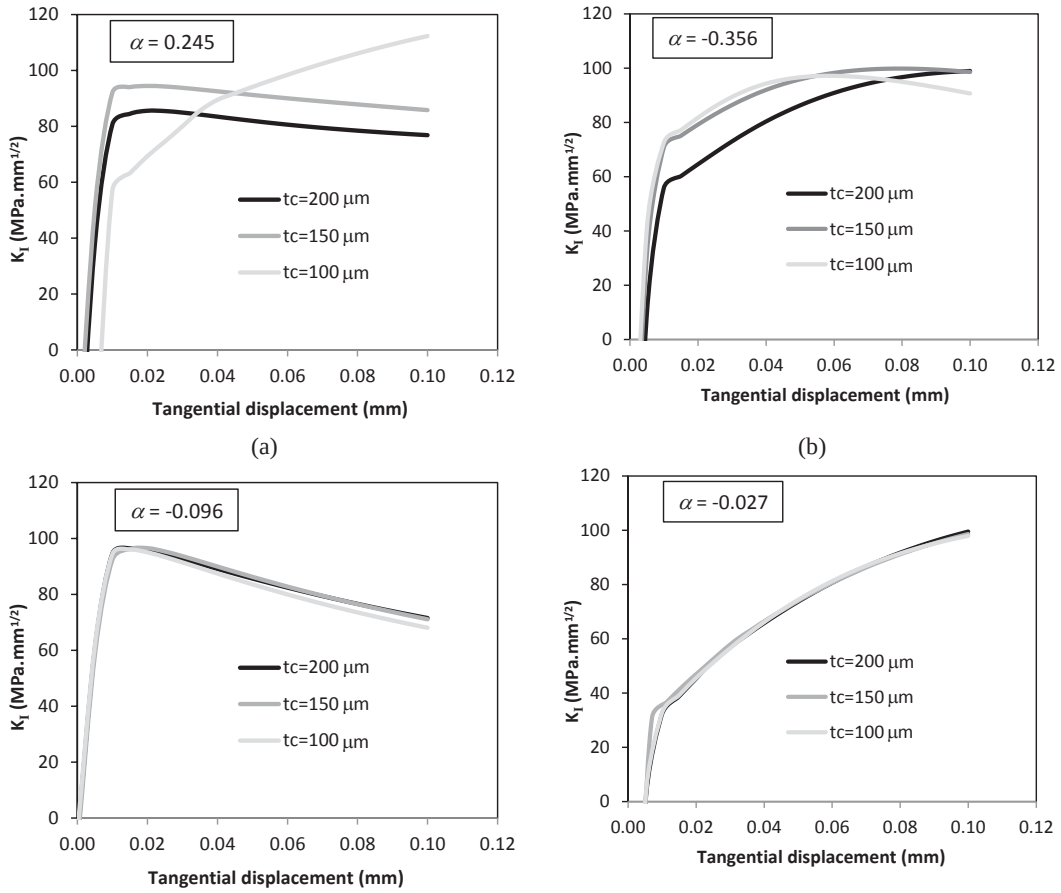

Fig. 12. Predicted K_I - displacement response from final propagated micro-cracks of Fig 7, for different coating thickness values and different Dundur's parameter values of coatings (a) α = 0.245, (b) α = -0.356, (c) α = -0.096 and (d) α = -0.027. (P = 500 N/mm, δ = 0.1 mm, μ = 0.3, K_{IC} = 100 MPa.mm$^{1/2}$).

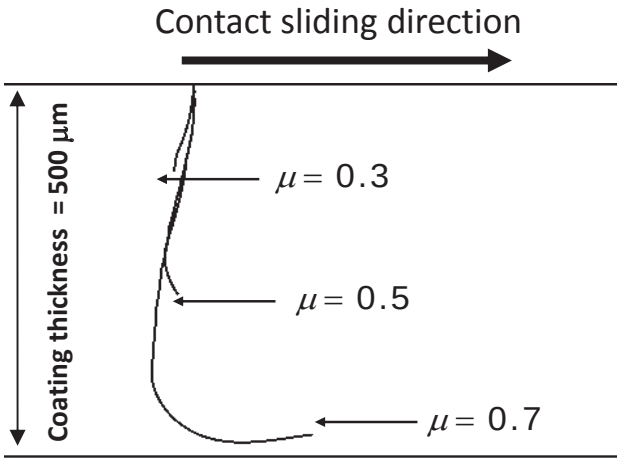

Fig. 13. Propagated crack profiles for different coefficient of friction, μ (α = -0.356, t_c = 500 μm, P = 500 N/mm, δ = 0.5 mm, K_{IC} = 126 MPa.mm$^{1/2}$), (Same scale is applied on vertical and horizontal axis).

Table(s)

Table 1. FE-based fast fracture model crack propagation prediction (P = 500 N/mm, δ = 0.1 mm, μ = 0.3, 100 MPa.mm$^{1/2}$).

coating/substrate	α, Dundurs parameter	β, Dundurs parameter	thickness (μm)	Max Contact pressure, P_{max} (MPa)	thickness/contact semi width	Crack propagate	final crack depth (μm)
Ec200/Ti-6Al-4V	0.245	0.036	100	1363	0.43	Yes	98
			150	1411	0.68	No	-
			200	1476	0.93	No	-
Ec100/Ti-6Al-4V	-0.096	-0.076	100	1243	0.38	No	-
			150	1218	0.57	No	-
			200	1203	0.74	No	-
Ec200/steel	-0.027	-0.053	100	1665	0.51	Yes	88
			150	1661	0.77	Yes	102
			200	1660	1.03	Yes	93
Ec100/steel	-0.356	-0.163	100	1453	0.43	Yes	50
			150	1366	0.61	Yes	70
			200	1316	0.80	Yes	89